Eur. Phys. J. A (2023) 59:179
https://doi.org/10.1140/epja/s10050-023-01093-6

THE EUROPEAN PHYSICAL JOURNAL A

Regular Article - Experimental Physics

Agata detector technology: recent progress and future developments

J. Eberth[1], H. Hess[1], P. Reiter[1,a], S. Bertoldo[2,3], C. Carraro[2], G. Maggioni[2,3], D. R. Napoli[2], W. Raniero[2], D. De Salvador[2,3]

[1] Institut für Kernphysik, University of Cologne, Zülpicher Strasse 77, 50937 Köln, Germany
[2] INFN-LNL, Viale dell'Università 2, 35020 Legnaro, Padova, Italy
[3] Dipartimento di Fisica e Astronomia, Università degli Studi di Padova, Via Marzolo 8, 35131 Padova, Italy

Received: 25 March 2023 / Accepted: 17 July 2023

Communicated by Nicolas Alamanos

Abstract γ-ray tracking is based on a new generation of position sensitive high-purity germanium (HPGe) detectors. A novel type of cluster detector was successfully developed and assembled for the high-resolution γ-ray spectrometer Advanced Gamma Tracking Array AGATA. The core part of the detector consists of three encapsulated, 36-fold segmented HPGe detectors which are operated in a common cryostat. The Ge crystal is hermetically sealed inside an aluminium can. All energy channels provide best energy resolution of core and segment signals for an extended energy range well above 50 MeV. A low cross-talk level was determined for the HPGe detectors and its preamplifier circuitry. Related cross-talk corrections are essential for highest energy resolution and improved position dependent pulse shape information. Recently a new encapsulation technology was put into operation which is based on a renewable metal elastic seal. HPGe detector developments are concerned with technologies for the production of p+ and n+ contacts, the segmentation and passivation of encapsulated HPGe crystals. Semiconductor processing research specifically aimed to develop a stable, thin and easy to segment n+ contact. A novel process, based on pulsed laser melting PLM, was successfully employed to produce very thin n+ and p+ contacts preserving the Ge purity. The contacts were segmented using a photolithographic process and then the intrinsic surface between contacts was passivated to assure the electrical insulation between them. A small detector prototype with three segments was made using these new techniques and then successfully tested.

1 Introduction

The new generation of γ-ray tracking spectrometers are the Advanced Gamma Tracking Array (AGATA) [1] in Europe and the Gamma-Ray Energy Tracking Array (GRETA) in the US [2–5]. AGATA and GRETA are so far the most advanced 4π-γ-spectrometers for nuclear structure research. It took almost 30 years to develop the technology [6] needed to build these detector arrays.

Part of this history is widely exposed in References [6, 7] and will be summarized in this introduction for the sake of completeness. The aim of this paper is twofold. First, to upgrade the description of technological advancements in segmented AGATA detectors (Sect. 2). Second to focus some remaining open questions about fabrication methodology and to report effective technological strategies to explore novel solutions (Sect. 3).

Hyperpure germanium (HPGe) was from the beginning the choice of detector material as it combines excellent energy resolution with good efficiency. The energy resolution is determined by the bandgap of Ge and the noise of the electronics. Resolution values of ΔE = 2 keV at 1.3 MeV were already achieved in early detectors. The efficiency was growing with time as larger and larger Ge crystals of hyperpure quality could be produced. Gamma rays which escape from the detector contribute to the background of the spectra. These events were suppressed by surrounding the Ge detector which BGO shield producing a veto signal. The 4π-arrays like GASP in Italy, EUROGAM (France/UK) and GAMMASPHERE in the USA exhausted the technology of escape suppressed Ge detectors. In these arrays nearly half of the solid angle was covered with the escape suppression shields and limited the total efficiency of the Ge detectors. In order to reduce this problem the idea of composite detec-

[a] e-mail: preiter@ikp.uni-koeln.de (corresponding author)

Published online: 03 August 2023

tors, with several closely packed Ge detectors mounted in the same cryostat, came up. This increased the efficiency by adding-back the Compton-scattered events between the detectors and enlarged the granularity for Doppler correction. The CLOVER detector [8] with four medium-sized Ge crystals was the first development of this type. The EUROBALL cluster detector [9] combined seven Ge detectors in the same cryostat. The shape of detectors was adapted to the icosahedron geometry of a tiled sphere, i.e. it had to be shown that Ge detectors of hexagonal shape could be produced without loss in energy resolution [10,11]. Furthermore, a hermetical encapsulation of the individual detectors [12] was developed in order to facilitate the production and the maintenance of large clusters of detectors.

The next step of the development was triggered by upcoming radioactive beam facilities. γ rays emitted after Coulomb excitation of radioactive beams exhibit usually large Doppler shifts as function of the observation angle. To correct for Doppler effects small opening angles or a high granularity of the detectors in the array are needed to avoid deterioration of the energy resolution. In first order this was solved by segmentation of the Ge detector contacts, e.g. 2-fold in part of the GAMMASPHERE detectors, 32-fold in the SeGA detectors at MSU [13]. Then a big progress was achieved by analysing the pulse shapes of all signals of a segmented detector in order to find the location of the interaction of the γ ray in the detector. For pulse shape analysis the signals of the preamplifiers are digitised and analysed online in a FPGA (see chapter on AGATA electronics of this topical issue). MINIBALL at Rex-ISOLDE, CERN [14,15], which became fully operational in 2001, was the first detector array of segmented Ge detectors operated with digital electronics for online pulse shape analysis. MINIBALL consists of 24 segmented Ge detectors arranged in 8 triple cryostats. The individual Ge detectors are longitudinally 6-fold segmented and hermetically encapsulated in an aluminum can. The MINIBALL detectors are not segmented along the Ge crystal axis. Therefore, the main interaction of the γ ray can only be determined in two dimensions by pulse shape analysis which is sufficient for Doppler correction.

The experience with MINIBALL and its digital electronics paved the way for approaching the final step: the development of the 4π-γ-ray tracking array AGATA (GRETA). The size of the Ge crystals was enlarged to 80 mm in diameter and 90 mm in length; the detectors were 36-fold segmented for optimum position resolution in three dimensions. Encapsulation of the sensitive, highly-segmented detector was essential for mounting and operating three AGATA or four GRETA detectors closely packed in the same cryostat. The 111 channels of an AGATA triple-cryostat are equipped with cold input stages of the preamplifiers. The input FET's and the feedback resistors and capacitors are mounted on the lid of the detector capsules cooled by copper braids which allows to operate the relevant analogue pre-amplifier electronics for minimum noise at a temperature of 130 K. This technology is optimised for best energy resolution, low crosstalk and low microphonics.

AGATA in its final configuration will be a highly efficient 4π γ-ray spectrometer consisting of 180 segmented HPGe detectors providing the high energy resolution typical for HPGe devices together with an outstanding detection efficiency. Moreover, the detectors will provide position information for the individual interaction energies and interaction positions of all γ rays within the segmented HPGe detector volumes [16]. The interaction positions of the γ rays within the individual segments of the HPGe detectors are obtained by means of Pulse-Shape Analysis (PSA) using different PSA methodes like e.g. the adaptive grid search [17]. All energies and coordinates of coincident interactions from PSA are then processed by a tracking algorithm. The tracking procedure will identify which energies and positions of these interactions belong together by determining the sequence they occurred.

In Sect. 2 of the paper we summarise the development of the composite AGATA Triple Cluster (ATC) detector which comprises three HPGe detectors operated in a common triple cluster cryostats. Within the cluster detector 111 individual spectroscopy channels are operated with cold input stages of all preamplifiers, that is advantageous for best energy resolution. Energy resolution measurements and crosstalk investigations were performed successfully meanwhile for twenty ATCs.

In Sect. 3 of the paper we present the latest advances in HPGe detector technology, aimed at improving the current segmented detectors, in particular in applications involving high radiation flux and high neutron-induced damage. As it will be explained in Sect. 3, these demanding working conditions will take a strong advantage if segmented future AGATA detectors could be made of p-type material with external n+ segmented contacts. A semiconductor process research was recently developed to identify a proper way to produce n+ thin and stable contact in HPGe. A new process, called pulsed laser melting (PLM), allows the production of very thin n+ and p+ contacts without jeopardising the hyper purity of germanium crystals. Segmentation of PLM contacts was implemented and proper surface passivation assured the correct performance of a small trial segmented detector.

2 AGATA detector configuration

The AGATA spectrometer consists of triple cluster detector modules. Each module comprises three encapsulated HPGe detectors with different hexagonal shaped crystals (see Fig. 1). The high efficiency and optimised solid angle coverage without suppression shields will be achieved by packing

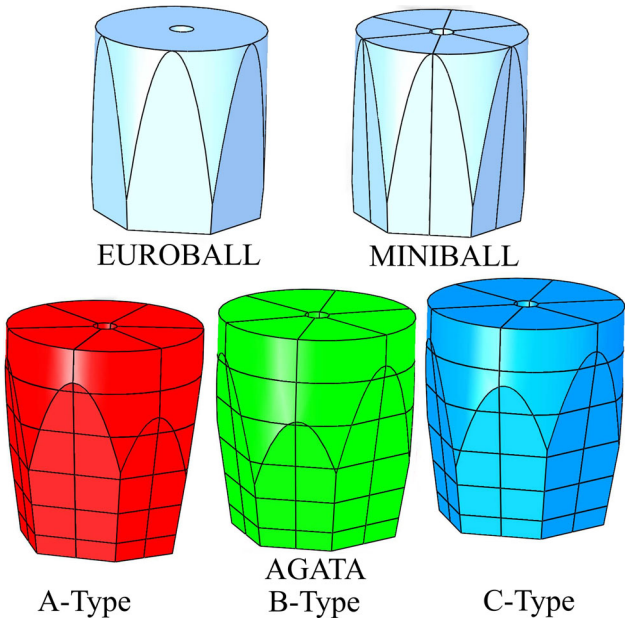

Fig. 1 Comparison of HPGe crystals employed for EUROBALL (unsegmented), Miniball (six-fold segmented) and AGATA (thirty six-fold segmented, three different shapes). The three types of AGATA crystals have slightly different side faces and tapering angles in relation with segmentation lines (see text)

the Ge crystals as close as possible inside the composite cluster detectors. Final constrains in solid angle and efficiency are given by the small distances between the Ge crystals and the surrounding aluminium material of the three encapsulated HPGe crystals and the common end cap of the cryostat.

The AGATA detector configuration is covering a high solid angle by tiling the surface of a sphere. In order to create a spherical shell with full 4π coverage an icosahedron geometry with 60 hexagons and 12 pentagons was chosen. Three HPGe detectors are combined in a common cryostat which is mounted in one of the 60 hexagons of the sphere. The three Ge crystals have a slightly different hexagonal shape in order to optimize the coverage with Ge. The 12 smaller pentagons are not filled with detectors. The ATC detector consists of three 36-fold segmented, hexagonal shaped, encapsulated tapered HPGe detectors. The individual HPGe crystals are hermetically sealed inside an aluminium can having thin walls and grouped inside the same cryostat. The detector configuration has an inner radius of 23.5 cm which allows the use of various ancillary detectors inside the target chamber. The HPGe detectors form a 9 cm thick germanium shell with $\approx 82\%$ of solid angle coverage.

2.1 Encapsulated HPGe detectors

The capsules of the EUROBALL, MINIBALL and AGATA detectors are built according to the same principles. The shape of the aluminum housing follows the shape of detectors which is hexagonal at the front end and circular at the rear side. The wall thickness of the can is 0.7 mm and the distance between the Ge crystal and the wall of the can is 0.3−0.7 mm. The cylindrical lid of the capsule contains the feedthrough for the high-voltage and the detector signals. Initially, the housing was hermitically closed with the lid by welding with an electron-beam under vacuum. The capsule is pumped through an Al tube which is closed by pinch-off. An activated getter material is mounted on the lid inside the capsule in order to maintain an ultra pure vacuum in the whole temperature range from the operating temperature of $\approx$ 85 K to the annealing temperature of 105 °C for removing a neutron damage of the Ge crystal. The getter material inside the encapsulated crystals is designed to keep a pressure below 10^{-6} mb for a period of 40–50 years. Two international patents were granted for the development of the encapsulation of Ge detectors [18,19].

In case of a problem with Ge detectors itself the welded capsule has to be opened by machining. It sometimes can be welded again but mostly the capsule parts are lost. To overcome this disadvantage a sealing technique using a metal-elastic seal has been developed which allows now to easily open and close the capsule many times without loss of parts. The seal is manufactured by the company HELICOFLEX. It is a flexible elastic metal seal that is compressed to achieve a vacuum tight sealing of the container for the HPGe crystal. The seal is composed of a close wound helical spring surrounded by a metal jacket. The spring is designed to have a specific compression resistance. During compression, the resulting pressure forces the jacket to fill the imperfections of the surfaces. Simultaneously tight contact with the flange sealing faces is ensured. The helical spring allows the seal to conform to surface irregularities on the flange surface. This technique facilitates the production and maintenance of encapsulated Ge detectors considerably. A picture of the reusable housing and the lid in shown in Fig. 2. A third patent was granted for this improvement [20].

2.2 AGATA cryostat

The triple cryostats have a length of 92 cm and a weight of 38 kg without the Ge crystals. Very low tolerances are demanded for the manufacturing of the cryostat end caps and the final spacing between detector side faces of different triple detectors.This is mandatory for precise positioning of the detectors in the array.

A narrow mechanical margin of 0.5 mm was achieved between end caps. The bending of the thin walls of the end-caps was measured to stay within tolerances under vacuum. The front part of the AGATA triple cryostat is shown in Fig. 3. The end cap is rendered semi-transparent to show the alignment of the detectors relative to the end cap. The picture also demonstrates one of the challenges in the design and

assembly of such a cryostat. A single triple cryostat comprises 111 individual high resolution spectroscopy channels. A comparable number of channels is typically employed in a full spectrometer like GAMMASPHERE.

The individual FET consumes an electric power of 20 mW, the total consumption of the 111 FETs in a single AGATA triple cluster adds up to 2.3 W. Together with the enhanced thermal connection by the wiring inside the cryostat and the radiative heat absorption, a considerable cooling capacity is demanded. The dewar for the triple cryostat contains up to 4.5 l of liquid nitrogen.

One dewar filling of liquid nitrogen is sufficient for 10–12 h of continuous operation. Temperature is monitored over two platinum resistance thermometer (type PT100) readouts. A PT100 is positioned at the copper cooling finger, close to the dewar and another PT100 is located in close vicinity of the crystals. A typical cooling down cycle of the ATC detector takes 8–10 h going from room temperature below -180°C. The temperature differences between the location of the PT100 close to the HPGe crystal and the actual temperature of the HPGe crystal is not accessible. Therefore, the cooling down period of the full triple cryostat assembly is prolonged over a period of 48 h in order to assure a temperature equilibrium which is very close to the measured PT100 values of typically 90–95 K.

A novel liquid nitrogen (LN_2) fill level meter has been put into operation for the all-position dewar of the ATC detector. The new device is based on a capacitance measurement between a metallic cylindrical tube inside the dewar and the inner wall of the cryostat. The fill level dependent capacitance is converted by a C/V-transducer into a DC voltage signal. Direct monitoring of the LN_2 level inside the detector dewar has been performed with several AGATA detectors at various inclinations and rotation angles of the detector axis. A calibration of the fill level capacitance measurement is performed for each dewar and its position in the array. A detailed description of the procedure is given in [21]. The time-dependent LN_2 consumption is an additional quantity used to survey the status of the cryostat. Supplementary results are the investigations of the LN_2 consumption and the heat loss of the detector during different modes of operation [21].

2.3 AGATA preamplifier

The pulse shape information is obtained from the time dependent charge collection process. The information is contained in the preamplifier output signals which should not be disturbed or affected by the electronic properties of the device. Advanced charge-sensitive feed-back preamplifiers were developed to achieve this goal employing fast reset technology for dead time and dynamic range optimization as well as a circuit structure for maximizing the open-loop gain of the charge-sensing stage.

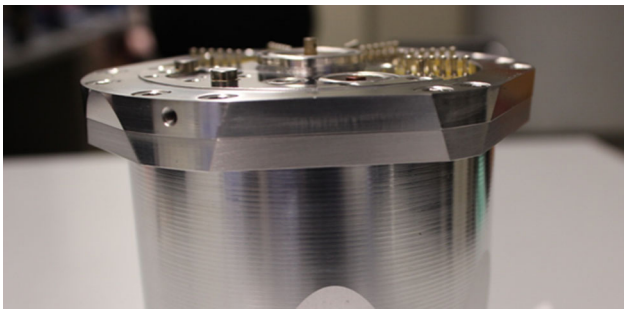

Fig. 2 The new encapsulation of the HPGe detector is based on a metal-elastic seal between the capsule lid and the crystal container. The delicate crystal can now be accessed in a replicable way by opening and closing the capsule in a controlled way

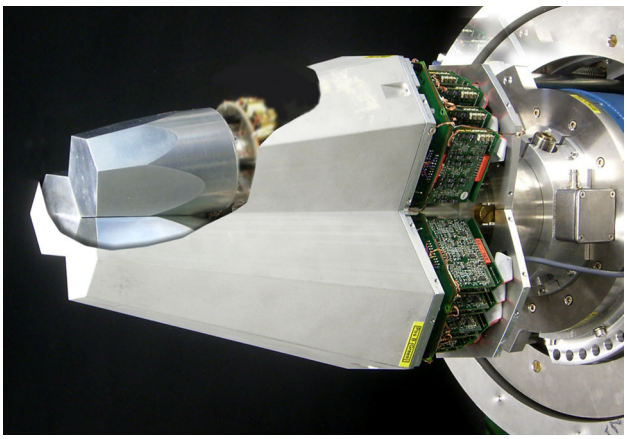

Fig. 3 The end cap of the AGATA triple cluster detector houses three thirty six-fold segmented encapsulated HPGe crystals of different shapes. The first feed-back loop of the preamplifier is located inside the cold part at very close distant to the crystals. Cooling with liquid nitrogen and very short signal paths minimise signal noise contributions. Picture provided by H.-G. Thomas, CTT, Montabaur

The preamplifiers are the only remaining analogue electronic parts which exist in the whole electronic measurement chain. To achieve highest energy resolution the preamplifiers of segment and core contacts are divided in two spatially separated parts. The cooled input stages of the preamplifiers are operated close to the Ge crystals (see Fig. 3). The AGATA cryostats employ a separate cooling for the encapsulated Ge detector and the cold part of the preamplifier electronics. While the Ge detectors are cooled to 90 K, the Field Effect Transistors (FET) are operated at temperatures near 130 K $\pm$ 20 K where their noise contribution is minimal. The other adjacent parts of the preamplifier electronics contribute less to the noise performance and are placed outside the vacuum. The cold part consists of a low-noise silicon FET, a 1.0 pF feedback capacitance and a 1 GΩ feedback resistance. A dedicated shielding was developed for the cold preampli-

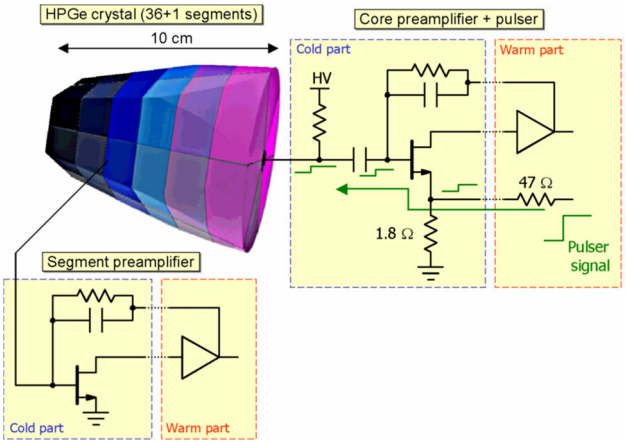

Fig. 4 Scheme of the core and one segment preamplifier. The signal path from the built-in pulser to the segments passes by a 1.8 Ohm resistor installed in the cryostat, the source of the jFET of the core preamplifier, the high voltage decoupling capacitor, and the detector bulk capacitance

fier board for minimizing the inter-channel crosstalk. The warm part, operated at room temperature, is located close to the cold part of the cryostat and comprises a low noise transimpedance amplifier, a pole-zero stage, a differential output buffer, and a fast-reset circuitry. Transient signals are not deformed due to the large bandwidth. The preamplifier development for AGATA is described in [22–24].

The segment and core signals of the AGATA detectors are read out simultaneously through advanced charge-sensitive resistive feed-back preamplifiers, employing a new fast reset technology for dead time and dynamic range optimisation as well as an original circuit structure for maximizing the open-loop gain of the charge-sensing stage. A custom programmable high-precision pulser located on the core-preamplifier board is used to inject calibration pulses to the core electrode itself as well as to all segment electrodes through the detector bulk capacitance, as shown schematically in Fig. 4. The main applications of the precision pulser are: testing, calibration, time alignment, efficiency measurements of the detector.

A novel reset scheme allows for an increased counting rate capability of the detector. In case a high energetic signal occurs in the detector, the output of the preamplifier goes in saturation and disables to process the next pulses. The desaturation circuitry is capable of detecting such signals upon which a current source is connected which discharges the capacity in the pole/zero network. A fast restoration of the output level is achieved allowing four to five times higher detection rates. Results of the novel Time-over-Threshold technique [24] for high resolution spectroscopy demonstrated a good energy resolution for an increased γ-ray energy range well above 50 MeV comparable with the standard pulse height mode.

A detailed description of the newly developed segment preamplifiers is given in [23]. Three segment preamplifier channels are integrated on one printed circuit board. The power consumption per channel is limited to 280 mW by design allowing the 111 closely packed spectroscopic channels to be operated close to the vacuum feed throughs in air between the cold part of the cryostat and the liquid nitrogen dewar (see Fig. 3). Differential signal output of the 111 spectroscopic channels are transmitted through 21 MDR cables.

2.4 Space charge in highly segmented HPGe detectors

The space charge distribution inside highly segmented large volume HPGe detectors were determined from capacitance–voltage (CV) measurements. For this purpose a computer code was developed to understand the impact of impurity concentrations on the resulting capacitance between core contact and outer contact for HPGe detectors, biased at different high voltages. The code is a tool for the reconstruction of the doping profile within irregularly shaped detector crystals. The results are validated by comparison with the exact solution of a true coaxial detector. The space charge reconstruction under cylindrical symmetry is derived. An extension of this scheme to higher dimensions for inhomogeneous space charge distributions is illustrated for a two-dimensional segmented coaxial detector [25]. The space charge distribution of a large volume highly segmented HPGe detector was determined by a non-destructive capacitance–voltage measurement. The capacitances between the 36 segments and the core were measured simultaneously with a precision pulser which was implemented in the core preamplifier. The pulser measurement was compared with and validated by direct capacitance measurements. The three-dimensional doping profile was reconstructed using analytical and numerical methods. Consistent values for the impurity concentration in the range of 0.5–1.5 $\cdot 10^{10}\,\mathrm{cm}^{-3}$ were obtained [26].

2.5 Energy resolution

At low γ-ray energies the energy resolution of the ATC is well within the following specification values. The energy resolution (FWHM) of the core contacts is $\leq$ 2.35 keV for E_γ = 1.33 MeV and $\leq$ 1.35 keV for E_γ = 122 keV. For the 36 segments, the resolution (FWHM) is $\leq$ 2.30 keV at 1.33 MeV (with a mean value of $\leq$ 2.1 keV) and $\leq$ 1.3 keV at 60 keV (with a mean value of $\leq$ 1.20 keV). Since the low energy resolution values are dominated by electronic noise, the obtained results demonstrate the successful design and integration of the new ATC detector. In particular the electronics properties comprising the cold and warm parts of the new preamplifier assembly is characterised by low noise in the triple cryostat despite the high integration density of 111 analogue channels. The improvement in the final assembly

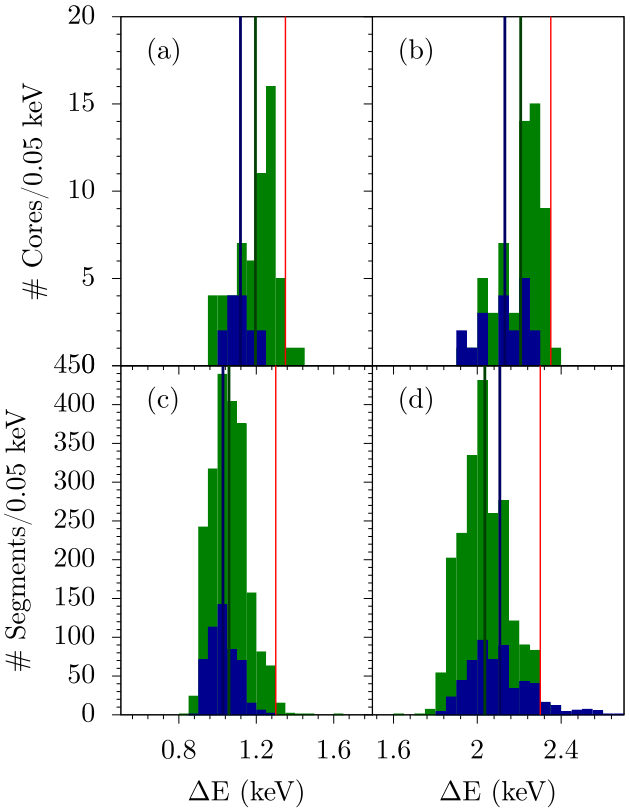

Fig. 5 Summary of energy resolution values (FWHM) of core signals (**a**, **b**) and segment signals (**c**, **d**) of 59 AGATA HPGe detectors (green bars). The energy resolution values are given for a γ-ray energy of 60 keV (^{241}Am) (**a**, **c**) and of 1.332 MeV (^{60}Co) (**b**, **d**). Several neutron damaged AGATA crystals went through the annealing procedure. The energy resolution values (FWHM) of HPGe detectors after annealing are also shown, (blue bars). The AGATA energy specification limits for both γ-ray energies are included as red lines. The mean values of the energy resolution for detectors after delivery are given as green line, the values for annealed detectors by blue lines (for details see text)

is a result of the new AGATA preamplifier and the grounding scheme in the ATC detector, which reduces unwanted perturbing high frequency noise contributions. A potential source for the microphonic effect at the core contact was removed by exchanging the coupling capacitor of the core signal from a foil capacitor to a ceramic capacitor and by a better fixing of critical cables..

The average energy resolution values of 59 AGATA HPGe detectors are shown in Fig. 5. The energy resolution values (FWHM) are given for a γ-ray energy of 60 keV (^{241}Am) and of 1.332 MeV (^{60}Co). At low energies the average of 2124 segment values are measured to be 1053 eV, while the average of 59 core values amounts to 1195 eV at the same energy. For the 1.332 MeV (^{60}Co) γ-ray energy, the average energy resolution of all segments is 2.03 keV while the core energy resolution is 2.21 keV. Meanwhile a couple of neutron damaged AGATA crystals went through the annealing procedure. The energy resolution values of these detectors are also included in Fig. 5. For low energies the segment energy resolution yields 1027 eV, the core value is 1117 eV. The mean energy resolution after annealing for 1.332 MeV (^{60}Co) is 2.11 keV for the segments and 2.13 keV for the core signals. All values from detectors after annealing are comparable, even slightly better, than the averages of new detectors. Over the years, the AGATA HPGe detectors have operated well within the specification for the energy resolution.

Built-in redundancies in highly segmented high-purity Ge detectors are exploited to increase the energy resolution of these semiconductor devices for detection of electromagnetic radiation in the X-ray and γ-ray regime. The information of the two electronically decoupled independent measurements, the cathode and the anode electrodes, provides an improved signal-to-noise ratio through a combination of the individually measured signals performed on an event-by-event basis. The average energy resolution values of the AGATA triple cluster detector for an energy deposition of 60 keV was measured to be 1.1 keV (FWHM) for the 36 segments and 1.2 keV for the core. The averaged signals of the core and the segments show an improved resolution value of 0.87 keV, which is close to the expected theoretical limit. At higher γ-ray energy the averaging technique allows for an enhanced energy resolution with a FWHM of 2.15 keV at 1.3 MeV. By means of the position sensitive operation of AGATA a new value for the Fano factor was determined and the noise contributions to the FWHM of a γ-ray peak separated [27].

The AGATA detectors are made of n-type HPGe detectors in order to be less sensitive to neutron damage than p-type detectors and due to the fact that large volume coaxial detectors can be constructed with thinner outer contacts. However, neutron damage is only reduced for the electron signal of the central core contact and not for the hole signals collected at the outer segments contact of the large volume detectors. Indeed, it was found that these segments are more sensitive to neutron induced traps than the core electrode during the first two experimental campaigns with the AGATA detectors at Legnaro and GANIL. The new HPGe crystals were exposed for the first time to the flux of fast neutrons from deep inelastic collisions, fission and fusion evaporation reactions. Fast neutrons are well known to produce specific lattice defects in germanium crystals which act as efficient hole traps. This causes a reduction in the charge collection efficiency of the detectors observable by a left, low energy tailing on the energy line shape.

The crystals can recover from neutron damage by annealing. Radiation damage to HPGe crystals can be repaired by warming up the HPGe crystal in the case of AGATA detector capsules to 105°C in an oven under vacuum conditions for typically three to seven days. The annealing restores the nominal HPGe lattice structure, removing charge trapping sites and thus restoring the energy resolution of the HPGe detec-

tors. After more than ten years of operation, many Ge crystals of the AGATA spectrometer passed through the annealing procedure. Up to now it was found that the mean values of the energy resolution is even slightly improved with respect to the new detectors (see results in Fig. 5).

However, for practical reasons and in view of the rate at which neutron damage becomes visible, this treatment cannot be applied after every experiment. Fortunately, pulse shape analysis is not influenced by neutron trapping: PSA is only sensitive to changes in the signal shape of the order of the one percent level, while the energy resolution is already sensitive below the per mill level. Therefore energy resolution will be deteriorated far earlier than it will be noticed in the PSA. Since the peak height deficiency will in first approximation only depend on the interaction position in the detector, the high position sensitivity of the AGATA array allows to make corrections for trapping effects using the precalculated trapping sensitivities. Such correction method was implemented for the AGATA detectors and are described in [28]. In the long term the AGATA collaboration intends to overcome the sensitivity of segment signals to neutron damage by the development of a suited p-type HPGe detector. First steps in these directions are already undertaken and are subject of the following Sect. 3

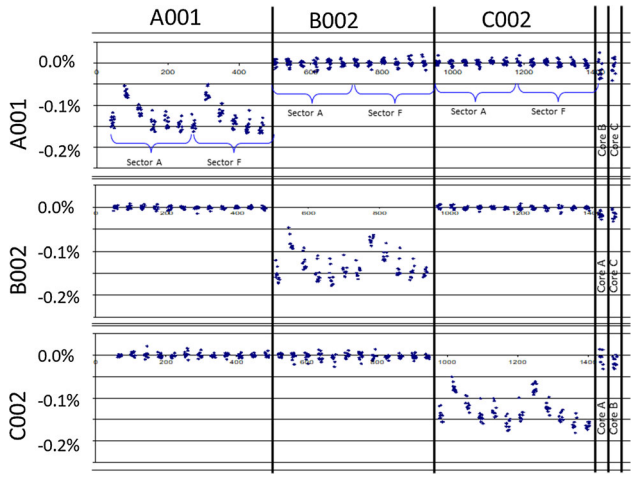

Fig. 6 Results of crosstalk measurements for detectors A001, B002, C002 in a common AGATA cryostat. For clarity only a subset of the 110×111 combinations of crosstalk matrix elements within the full triple cryostat is shown from the sectors A and F of each detector. On the diagonal graphs the crosstalk pattern within each single detector is of the 0.1% level. The observed structures can be entirely attributed to the capacitive coupling between core and segments. The crosstalk contributions between different detectors is shown in the six off-diagonal graphs. No indication for crosstalk contributions appear between segments of different detectors at a level $\leq 10^{-5}$. The results are based on a novel method for determination of precise and absolute crosstalk matrix elements [29,30]

2.6 Crosstalk properties of highly segmented HPGe-detectors

Crosstalk properties of 36-fold segmented, symmetric, large volume, HPGe detectors from the AGATA collaboration were deduced from coincidence measurements performed with digitised segment and core signals after interaction of γ rays with energies of 1.33 MeV. The mean energy values measured by the core signal fluctuate for γ-ray interactions with energy deposited in two segments. A regular pattern is observed depending on the hit segment combinations. The core energy shifts deviate 0.03–0.06% from the average energy calibration. The segment-sum energy is reduced with respect to the core energy as a function of the decoupling capacitance and the segment multiplicity. The deviation of the segment-sum energies from multiplicity two events fluctuates within an interval of less than 0.1% depending on the different segment combinations (see Fig. 6). The energy shifts caused by crosstalk for the core and segment signals are comparable for all three shapes of detectors. A linear electronic model of the detector and preamplifier assembly was developed to evaluate the results. The fold-dependent energy shifts of the segment-sum energies are reproduced. The model yields a constant shift in all segments, proportional to the core signal. The measured crosstalk pattern and its intensity variation in the segments agree well with the calculated values. The regular variation observed in the core energies cannot be directly related to crosstalk and may be caused by other effects like electron trapping [29].

The crosstalk effects cause shifts in the measured γ-ray energy of the core and segment signals as function of segment multiplicity. The positions of the segment sum energy peaks and their resolution deteriorates vary approximately linearly as a function of segment multiplicity. Two methods were developed to correct for the crosstalk induced effects by employing a linear transformation. The matrix elements are deduced from coincidence measurements of γ rays of various energies as recorded with digital electronics. A very efficient way to determine the matrix elements is obtained by measuring the base line shifts of untriggered segments using γ-ray detection events in which energy is deposited in a single segment. A second approach is based on measuring segment energy values for γ-ray interaction events in which energy is deposited in only two segments. After performing crosstalk corrections, the investigated detector shows a good fit between the core energy and the segment sum energy at all multiplicities and an improved energy resolution of the segment sum energy peaks. The corrected core energy resolution equals the segment sum energy resolution which is superior at all folds compared with the individual uncorrected energy resolutions. This is achieved by combining the two independent energy measurements with the core contact on the one hand and the segment contacts on the other hand [30].

The crosstalk properties of a complete asymmetric triple cluster detector were investigated by events from source measurements with only one detector segment collecting a real energy deposition in the detector volume. All traces were recorded whenever one channel triggered. In coincidence with the energy information of the triggering segment the baseline shift in all other segments are recorded as a function of the energy deposition in the hit segment. The equivalent energy ratio, corresponding to these baseline shifts in the untriggered segments, is of the order of $\approx 10^{-3}$ and follows linearly the energy deposition. The measurements were performed with one of each of the three AGATA shaped detectors in a common AGATA cryostat The pulses from all 107 remaining segments without trigger condition are recorded and analysed simultaneously with the pulse from the hit segment. After identification of the true energy deposition in exactly one segment the coincident and simultaneous baseline shifts are recorded which occur in all remaining 107 non-hit segments. This method allows determination of precise and absolute crosstalk matrix elements. The details are published in [29,30]. The crosstalk pattern within each single detector is of the 0.1% level as shown in Fig. 6 for two sets of sector signals. The observed structure in the three diagonal parts of Fig. 6 can be entirely attributed to the capacitive coupling between core and segments. A repeating pattern was observed for the segment signals within the same HPGe detector caused by the interplay of the core coupling capacitor and the distinct different capacitances of the 6 segments along one ring in the detector. The measured values are shown in parts for the extended 108×108 matrix Fig. 6. A negligible cross talk level below 10^{-5} was found between core and segment signals of detectors that are not hit by γ radiation (see six off-diagonal panels and values for the core coupling in Fig. 6).

In summary, crosstalk properties of the highly packed analog preamplifier circuitry and detector assembly does not induce crosstalk between different detectors. A negligible cross talk level below 10^{-5} was found. An expected low and regular crosstalk level of 10^{-3} was observed for the segment signals within the same HPGe detector caused by the interplay of the core coupling capacitor and the capacitances of the 36 segments.

3 Advances in detector technologies

There are still several aspects of segmented position sensitive Ge detectors for tracking arrays, which need to be developed and/or improved. The limitations on the key HPGe segmentation technologies are particularly relevant. Among the various possibilities, available from microelectronics technology, to produce p+ (holes collecting) and n+ (electron collecting) junctions, only a few of them preserve the needed net impurity concentration of the high-purity germanium detectors as low as $\approx 10^{10}\text{cm}^{-3}$ after the production process [31]. As mentioned in Sect. 2.5, the AGATA detectors produced so far are based on the ion implantation of boron at room temperature for the p+ contact and on the diffusion of lithium at 300 °C for the n+ contact. The high diffusivity of Li in Ge produces a very thick junction in the order of 0.5−1.0 mm with many detrimental effects: (i) it is a dead layer where no charge collection occurs [6], (ii) is not stable under annealing treatments required for damage recovery, causing loss of active detection volume [32], (iii) and prevents stable and thin segments.

The segmentation is currently performed on the p+ boron side, that has a junction depth of about 300 nm and can be easily divided into insulated contacts. These technological limitations force the use of holes h+ signals on the segments to build the tracking analysis. However, it is known that holes are much more subjected to trapping induced by neutron damage, with a detrimental effect on the resolution [33] that develops at a 30 times lower dose with respect to electrons [34].

At present, most spectrometers like AGATA, GRETA, GAMMASPHERE, GALILEO and GASP are therefore built out of hole-collecting n-type bulk Ge material with external boron implanted segmentable contacts. This causes the segments to be subjected to neutron damage and requires for periodic thermal annealing procedure as described in Sect. 2.5. Moreover, to extend as long as possible the time between annealings, often the central segment signal is collected to correct the energy resolution of the gamma events. A polarity inversion of the coaxial segmented detector, i.e. working with a p-type bulk and external electron collecting segments, would have in principle two advantages: (i) an extension of the time-span between successive annealings, allowing to reduce the operational cost, or giving the possibility to work under more neutron damaging conditions; (ii) in principle, the collection of the central signal would not be necessary anymore to correct the energy resolution. In this way γ-ray interactions can be distributed with higher frequencies on different segments, allowing to increase the counting rate. However, annealing is still expected, albeit after a higher neutron dose than before. Therefore, the n+ contact has to be thermally stable (i.e., annealable) beside being thin to allow for an easy segmentation. Such kind of contacts do not seem to be available at the moment, since they can not be performed by actual lithium diffusion processes, nor with amorphous contacts that are demonstrated to be not stable under annealing. The need for new contact technology appears to be a relevant issue in order to realise performance improvements in terms of radiation hardness and counting rate.

A recent and promising progress in this field was obtained by LNL-INFN in the framework of the CSNV PRONG (Pro-

cesses for Next Generation Gamma Germanium detectors) project. For the first time the pulsed laser melting (PLM) process was tested to produce n+ and p+ doped junctions in HPGe gamma detectors. Here the main aspects of this process will be presented.

3.1 Bulk contamination during doping processes

The introduction of new doping processes producing stable and thin junctions is a mandatory step in order to have electron collecting segmented contacts less prone to neutron damage. The first thing to be evaluated for any new process in HPGe is that the high purity level of germanium must be preserved. This property plays a crucial role, since it makes it possible to create large depletion regions, i.e. large interaction volumes. High purity Ge has less than one impurity atom per trillion crystal atoms. This purity level is easily jeopardised by contaminants like e.g. Cu, which is the most common, diffusing from the environment to the bulk. Lithium evaporation step involved in the formation of the actual n+ junctions must be performed at about 300–400°C and is generally considered as an upper limit for thermal treatments before having irreparable contaminations of the bulk.

In a recent paper Boldrini and co-workers [31] systematically investigated the thermal budget limit for HPGe contaminations. Several HPGe samples were treated by different doping and thermal processes and then the contaminations of the bulk were investigated by means of van der Pauw–Hall electrical measurements. In Fig. 7 bulk charge density measured after processing is presented for different treatments as a function of temperature inverse. At high temperature (low 1/T) the typical exponential growth of thermal carriers is present. At low temperature the carriers due to residual bulk doping are visible. The starting materials are either p-type or n-type HPGe and show a background doping of less than 10^{10}cm^{-3} (full and empty black squares, respectively).

All the data from blue downward triangles to brown upward triangles are the results of different thermal processes. For all these processes temperature and time duration are reported. Where "SOD" is reported, it means that the samples have been deposited with a Spin ON Dopant (SOD) layer before the process in order to induce a thin junction on the surface of the layer [35]. It is worth noting that the reported carrier concentration is obtained after removal of the thin layer and gives a measure of the bulk contamination induced by the process. Where only time and temperature are reported, a simple thermal cycle was performed without SOD deposition. All the processes were performed in a tubular furnace within a quartz vessel under 10^{-6} mbar, except for RTA process for which a Rapid Thermal Annealing (RTA) apparatus was used [35]. The background doping of the bulk is always worse than the starting level, moreover it is always

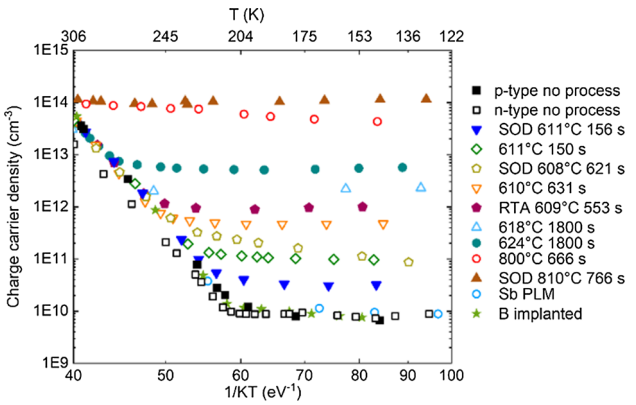

Fig. 7 Charge-carrier density curves as a function of $1/k_BT$. Full symbols refer to p-type starting substrates, empty symbols refer to n-type substrates

a p-type dopant, even when the starting material and/or the doping process is n-type.

The data were elaborated by means of a phenomenological model that introduces the concept of thermal budget, TB, as the integral of an exponentially activated contamination process over the time, i.e. along the thermal history (temperature T as a function of time t) of the sample:

$$TB = \int exp\left(\frac{-E_{act}}{k_B T(t)}\right) dt \tag{1}$$

where k_B is the Boltzmann constant and E_{act} is the activation energy of the contamination process. Contamination concentration (n) of experimental data is correctly reproduced by the following equation: $n = A \cdot TB$ with $A = 2.1 \cdot 10^{21} cm^{-3} s^{-1}$ and E_{act} (activation energy) equal to 2.1 eV.

This simple model shows that conventional diffusion based doping methods are not suitable to produce contacts on HPGe. In practice, the diffusion process of most common dopants (i.e. Sb, P, Ga) is too low and, while the junction forms, bulk contamination occurs. The data are compatible with the known diffusion mechanism of Cu, that is a very-fast-diffusing, p-type dopant. Lithium doping appears to be the only exception among the diffusion doping methods, since its interstitial diffusion is fast and can compete successfully with that of Cu.

In Fig. 7 the only surface doping processes that preserve the purity are B implantation at room temperature (green stars), that does not need any thermal budget to be electrically activated, and Pulsed Laser Melting process (light blue circles). This last process, described in more detail in the following section, is a very fast process that causes a melt of the surface for a limited time (about hundred nanoseconds). The thermal budget is therefore very limited, but diffusion of standard dopants may occur since diffusion coefficient is consistently higher in liquid than in solid.

3.2 Laser doping of Ge

PLM is a particular annealing process in which a UV pulsed laser is used as heat source. When the sample is irradiated with one or multiple laser impulses, the UV photons of each impulse are absorbed in the first few nanometers of the Ge surface, promoting electrons from the valence to the conduction band. The electrons decay immediately by means of intra-band transitions, transferring energy to the crystal lattice. The generated heat diffuses for a few hundred nanometers, leading to melting of the layer, while leaving the bulk nearly at room temperature. During the melting time, if a dopant element is present at the surface, it can in-diffuse very fast due to very high diffusivity in liquid, that is about five orders of magnitude higher than in solid. Finally, the layer recrystallizes once the heat is dissipated. The recrystallisation is a very fast liquid phase epitaxy, leaving a coherent reconstructed crystal with high incorporation of dopant. Due to the out-of-equilibrium dynamics, an incorporation of dopant well above the solid solubility can be reached [36,37]. In case laser pulses are applied for a few nanoseconds, the whole process is carried out in a few hundred nanoseconds, resulting in a very low thermal budget. Bulk contaminations of HPGe material are therefore avoided, as demonstrated in the previous Sect. 3.1.

As stated, some of the major limitations in the production of segmented detectors with electron collecting contacts are connected to the absence of a junction formation methodology that provides thin and thermally stable contacts without contaminating the bulk.

The combination of PLM processes and thin layer depositions, such as sputtering, could prove useful to overcome such limitations, as they represent a way to obtain thin doped layers with tunable and controlled thickness and high doping levels [38]. Indeed, the thickness of the PLM molten layer depends strongly on the energy density of the laser pulse itself, while the thickness of the initially deposited layer is directly connected to the dopant dose. Furthermore, such a combination allows to overcome other technological issues connected to traditional doping techniques, as honeycomb structures and lattice damages due to dopant implantation [39], or low dopant activation in in-situ doped layers [40]. The new approach has been studied using Sb as n-type dopant on a Ge wafer [41] achieving promising results. In this study, metallic Sb layers with thicknesses ranging from 8 nm down to a single monolayer were deposited on the surface of the Ge wafer to create a dopant source for the following laser process.

The device used for PLM was an excimer laser (Coherent COMPex 201f), emitting light at $\lambda = 248\,\text{nm}$ over a square spot $5 \cdot 5\,\text{mm}^2$ with tunable energy density and 22 ns impulse duration. With the first laser impulse, the Sb layer is incorporated in the germanium lattice during the melting phase of PLM. When multiple laser impulses with the same energy density are applied, the dopant atoms distribute repeatedly in the same layer with fixed melt depth, resulting in box-like depth profiles, shown in Fig. 8. The performed PLM processes produce samples with dopant atoms confined in the recrystallized layer, in concentrations as high as $5 \cdot 10^{21}\,\text{at}/cm^3$, which are well above the solid solubility limit (around $10^{19}\,\text{at}/\text{cm}^3$ in the case of Sb).

The resulting doped layers have been extensively characterised, showing excellent properties, regarding both electrical activation, crystallinity and lattice coherence between layer and bulk (pseudomorphicity). The obtained junction is nearly 150 nm thick, with chemical concentrations that reach 10% of the substrate density and show no segregation. Only a fraction of the dopant is active, nonetheless the active concentration reaches a notable $3 \cdot 10^{20}\,\text{at}/\text{cm}^3$. The layers are pseudomorphic to the substrate and show no extended defects. These are promising characteristics for the formation of n+ contacts for future detectors.

Since PLM method is an epitaxial procedure, it is important to understand how the process depends on the lattice orientation. Planning to apply the process to complex geometries such as coaxial detectors, the doping should successfully occur along surfaces with different orientations. In order to clarify this point, the combination of sputter deposition and PLM was used on Ge wafers with (100), (110) and (111) crystallographic orientations. All the samples received a 2 nm thick Sb sputter deposition and were subjected to 1–4 laser impulses at $500\,\text{mJ}/\text{cm}^2$ energy density. The chemical and active dopant depth profiles of the resulting doped layers are reported in Fig. 8 and confirm that a very thin junction of nearly 150 nm is formed in all samples. The active concentration is also notable, around $3 \cdot 10^{20}\,\text{at}/\text{cm}^{-3}$ for every orientation. Finally, the crystallographic orientation does not seem to play any role in the dopant diffusion, nor in its activation, suggesting that this process could be successfully implemented on the lateral surfaces of coaxial crystals as well.

As far as acceptors are concerned, these same processes have also been studied using Al as p-type dopant. Considering its sensitivity to oxygen, a protective amorphous Ge cap was deposited on top of the Al layer prior to laser irradiation. During PLM the two layers merge and diffuse in the substrate lattice, resulting in a thin highly doped junction. This study is the object of an approved patent [42]. In reference [43] the n-type PLM doping procedure described above was successfully applied to produce a first test detector of $10 \cdot 10 \cdot 2\,\text{mm}^3$ size. The detector shows a very good resolution less or equal to 1 keV in the range from 50 to 400 keV. A further step to validate the methodology is to demonstrate the feasibility of segmentation of a PLM contact. This aspect will be discussed in the following section.

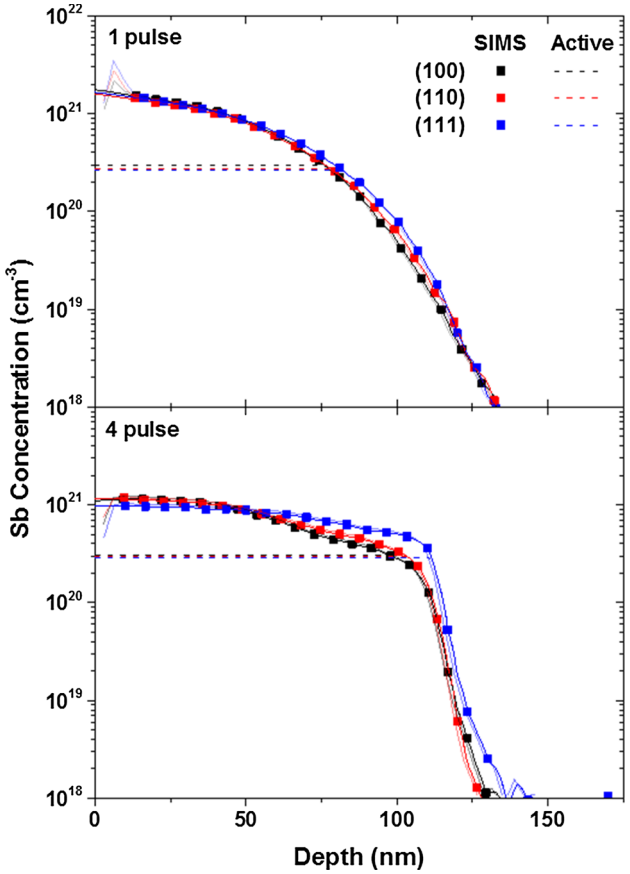

Fig. 8 Sb chemical depth profiles as measured by Secondary Ion Mass Spectrometry on Ge wafers with different crystallographic orientations after a 2 nm thick Sb sputtering deposition and one (top panel) or four (bottom panel) KrF laser impulses at 500 mJ/cm^2. The profiles were extrapolated in the first 20 nm toward the surface to avoid SIMS transient effects (raw profiles in blurred lines). The corresponding active dopant profiles are shown in dashed lines

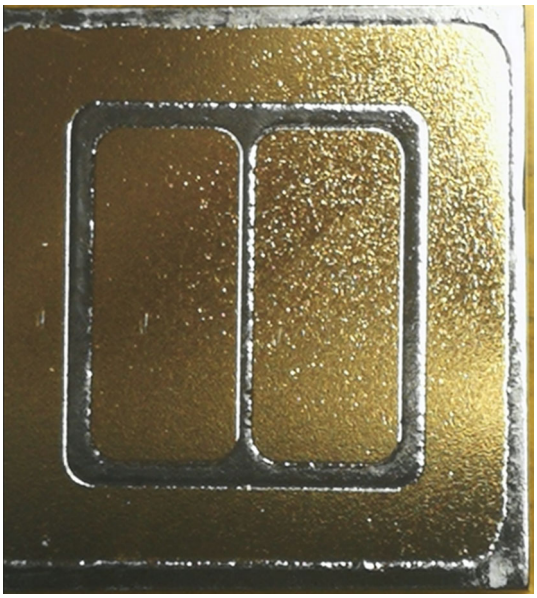

Fig. 9 Protype p-type HPGe detector $10 \cdot 10 \cdot 2$ mm^3 after PLM on the Sb junction, gold plating, photolithography and passivation

3.3 Segmentation of PLM contacts

The segmentation of the outer contact of a coaxial detector is one of the most important steps to ensure proper PSA for tracking arrays. N-type detectors with Boron outer junctions are segmented by producers using proprietary techniques. On the other hand, p-type coaxial crystals with outer Lithium thick junction can be mechanically segmented by dicing techniques, with the consequent introduction of lattice defects [44,45]. With the PLM technique, thin junctions are available for both charge carriers, hence a less invasive segmenting step, like photolithography, can be introduced. Recently a photolithographic process was used in a study, which developed a trial segmented HPGe planar detector (Fig. 9) [46,47].

In order to separate several contacts on a continuous PLM junction, a 100 nm Au layer is first sputtered on the doped Ge as a metal contact. The sample is then spin coated with a positive photoresist to cover the metal contact with 1–2 μm thick photosensitive layer and baked to promote crosslinking: a good compromise for the resist thickness is found considering that thinner films lead to higher resolutions, but also to stricter parameters for the subsequent processes. A mask is then aligned on the sample to impress a specific geometry on the resist: the mask is generally a high-resolution image with black areas reproducing the electrical contacts drawn on a UV-transparent acetate or chrome-gold etched depositions on quartz glass. A considerable contribution to the final lithographic resolution is evidently given by the resolution of the shadowing image and the UV light collimation. The resist is exposed for a time sufficient to break crosslinks between molecules, but not excessive to avoid overexposure, which can drastically reduce resolution. The exposed sample is then rinsed in developers, usually hydroxides, several times to ensure the removal of the exposed resist, baked again and submerged in gold etchant to remove the metal layer in the regions between contacts. The remaining photoresist is then removed in organic solvents. The detector is finally etched with a hydrofluoric-nitric acid mixture to dig a trench between the contacts, removing several microns of germanium where the gold layer was etched: this acid does not react with Au and, thanks to the shallow highly doped junction, this results in electrically separated junctions. A final chemical step of passivation (consisting in a hydrofluoric-nitric acid etching quenched in methanol [48]) has been applied just after the etching to get electrical insulation of the surfaces that are not protected by gold.

The trial segmented detector was tested both with diode current–voltage characteristics curves (for both segments) and with spectroscopic measurements. A ^{133}Ba source was

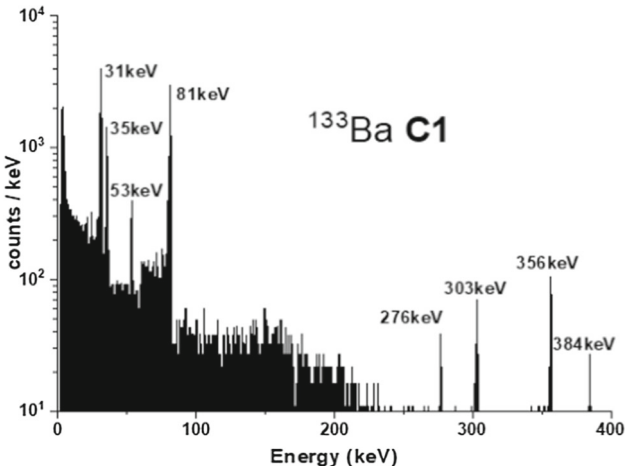

Fig. 10 ^{133}Ba spectra at 20 V polarisation voltage for the left segment C1 of the 2 mm thick detector in Fig. 9

used to measure counting rates and energy resolutions (FWHMs) at several energies: 30 keV and 35 keV photopeaks are clearly visible and well separated and FWHMs for 81 keV photopeak in both segments are 0.73 keV, confirming a high resolution for this device (data for the left segment are shown in Fig. 10). The four photopeaks at higher energies show low counting rates because of the small active volume of this device. The same detector was then annealed at 100 °C for 40 h to simulate a typical recovery annealing that could be performed after neutron damage and the measurements were repeated. FWHMs for 81 keV photopeaks did not change, showing that the annealing process does not compromise the device's performance.

With this full photolithographic process, the granularity of the contacts can be reduced to a level limited only by the wire bonding dimensions or by available computational resources. The techniques described for planar detectors can be transferred to coaxial detectors with the aid of spray coating resists and focused laser diodes exposures.

3.4 Surface passivation of HPGe detectors

Reverse bias at high voltages assures the charge depletion of the whole volume of a HPGe detector and the suppression of bulk currents in between the n and p contacts, but involves the passivation of the intrinsic surface between the contacts in order to avoid surface leakage currents. Surface passivation is also necessary in between segments of a segmented HPGe detector. Unfortunately, unlike SiO_2 Ge oxides are neither chemically nor thermally stable and then are not suitable for long-term passivation.

In the commercially available detectors, proprietary passivation layers (e.g. sputtered SiO_2, a-Ge and a-Si) are used, whose dielectric performance is suitable for charge collection from the full active volume of the detector. However, these layers can modify the electric field configuration near the surface and give rise to the formation of thick dead layers, where charges are lost or delayed beyond the typical charge collection times [6]. This problem can be particularly serious in AGATA detectors, where every location in the crystal is important for γ-ray tracking. For these reasons, several methods for Ge surface passivation have been investigated in the last years. Very good results have been obtained with methanol passivation, hydride and sulphide termination [48–51] and deposition of thin layers of Ge nitrides and oxynitrides [52–54]. As compared with commercial passivation, the dead layers produced by methanol passivation and hydride termination are much thinner and more homogeneous, assuring successful inhibition of inter-electrodes leakage currents, even at high potential gradients ($\geq$ 1 kV/cm) [49].

These alternative passivations do not display an acceptable stability in thermal and vacuum cycles that go from cryogenic to annealing temperatures (around 100°C), owing to their low resistance to oxidation and hydration [50]. However, the resistance of all these passivations can be strongly improved by the application of a protective coating obtained by means of a vacuum deposition process [55]. In addition to improving the passivation resistance both during the annealing cycles and during the maintenance and repair phases, in which the detectors are exposed to the atmosphere, the protective coating can preserve the detector surface from accidental damage both during detector operation and handling.

4 Conclusion

The development of position-sensitive, encapsulated Ge detectors represents a new quality in high-resolution γ-ray spectroscopy. It enabled the realisation of γ-ray tracking arrays like AGATA and GRETA which enhance the sensitivity for the investigation of rare events by two orders of magnitude over the former Compton-escape suppressed Ge detector arrays. AGATA is increasing in the numbers of detectors towards 4π. At this time it is one third of the 4π array and it is operational at the Laboratori Nazionali di Legnaro.

The encapsulation technology improved the reliability of Ge detectors and their annealing of radiation damage considerably, such that for more than 20 years this technology is applied in most space missions with Ge detectors. Furthermore Compton-cameras with position-sensitive Ge detectors have an interesting potential for application of imaging methods in medicine, nuclear waste disposal and homeland security.

So far, the main emphasis of the AGATA detector development was the encapsulation and segmentation of n-type, coaxial HPGe detectors with outer Boron-implanted p^+-contact and Lithium diffused n^+-contact at the inner bore-

hole. We discussed the possible advantages of having external n+ segmented detectors with p type bulk and inner p+ contact. This would in principle allow for higher radiation hardness and higher counting rate. However, progress in the n+ contact processing on HPGe has to be finalised, to realise such a detector. We showed promising recent results to this showing how pulsed laser melting technique can produce thin, segmentable n+ and p+ contacts without inducing bulk contaminations. Moreover, we demonstrated the feasibility of the process on different crystalline structures and the good performance retained after annealing. Work is in progress to demonstrate the scalability of the process to large coaxial crystals.

Acknowledgements The continuing long cooperation with the AGATA collaboration, in particular with the members of the AGATA detector working group, is gratefully acknowledged by the authors. J.E., H.H. and P.R. acknowledge an ongoing fruitful and constructive cooperation with the companies CTT, Montabaur Germany and Mirion Technologies (Canberra) France SAS. The authors thank H.-G. Thomas (CTT, Montabaur) for providing Fig. 3 of the ATC. This research was supported by the German BMBF under Grants 06K-167, 06KY205I, 05P12PKFNE, 05P15PKFN9, 05P18PKFN9 and 05P21PKFN9. AGATA was supported by the European funding bodies and the EU Contract RII3-CT-2004-506065. Funding was received from the grant agreement n. 262010 (ENSAR), from the European Union's Horizon 2020 research and innovation programme under grant agreement n. 654002 (ENSAR2).

Funding Open Access funding enabled and organized by Projekt DEAL.

Data Availability Statement This manuscript has no associated data or the data will not be deposited. [Authors' comment: The experimental data of this work related to Sect. 1 are available upon reasonable request by contacting the corresponding author. The experimental data related to Sect. 2 will not be deposited.]

References

1. S. Akkoyun et al., Nucl. Instrum. Methods A **668**, 26 (2012)
2. GRETA/GRETINA Website. https://greta.lbl.gov/home. Accessed 2022-09-21
3. M. Deleplanque, I. Lee, K. Vetter, G. Schmid, F. Stephens, R. Clark, R. Diamond, P. Fallon, A. Macchiavelli, Nucl. Instrum. Methods Phys. Res. Sect. A: Accelerat. Spectrom. Detect. Assoc. Equip. **430**(2), 292 (1999). ISSN 0168-9002. https://www.sciencedirect.com/science/article/pii/S0168900299001874
4. K. Vetter, Nucl. Phys. A **682**(1), 286 (2001). ISSN 0375-9474. https://www.sciencedirect.com/science/article/pii/S0375947400006527
5. I.Y. Lee, M.A. Deleplanque, K. Vetter, Rep. Prog. Phys. **66**(7), 1095 (2003). https://doi.org/10.1088/0034-4885/66/7/201
6. J. Eberth, J. Simpson, Prog. Part. Nucl. Phys. **60**(2), 283 (2008). ISSN 0146-6410. https://www.sciencedirect.com/science/article/pii/S0146641007000828
7. K. Vetter, Annu. Rev. Nucl. Part. Sci. **57**(1), 363 (2007). https://doi.org/10.1146/annurev.nucl.56.080805.140525
8. G. Duchêne, F. Beck, P. Twin, G. de France, D. Curien, L. Han, C. Beausang, M. Bentley, P. Nolan, J. Simpson, Nucl. Instrum. Methods Phys. Res. Sect. A: Accelerat. Spectrom. Detect. Assoc. Equip. **432**(1), 90 (1999). ISSN 0168-9002. https://www.sciencedirect.com/science/article/pii/S0168900299002776
9. J. Eberth, H. Thomas, D. Weisshaar, F. Becker, B. Fiedler, S. Skoda, P. Von Brentano, C. Gund, L. Palafox, P. Reiter et al., Prog. Part. Nucl. Phys. **38**, 29 (1997). ISSN 0146-6410. 4 pi High Resolution Gamma Ray Spectroscopy and Nuclear Structure. https://www.sciencedirect.com/science/article/pii/S0146641097000033
10. J. Eberth, P. von Brentano, W. Teichert, T. Mylaeus, R. Lieder, W. Gast, G. Hebbinghaus, H. Jäger, K. Maier, H. Grawe et al., Nucl. Phys. A **520**, c669 (1990). ISSN 0375-9474, nuclear Structure in the Nineties. https://www.sciencedirect.com/science/article/pii/037594749091183R
11. J. Eberth, P. Von Brentano, W. Teichert, H. Thomas, A. Werth, R. Lieder, H. Jäger, H. Kämmerling, D. Kutchin, K. Maier et al., Prog. Part. Nucl. Phys. **28**, 495 (1992). ISSN 0146-6410. https://www.sciencedirect.com/science/article/pii/0146641092900513
12. J. Eberth, H. Thomas, P. Brentano, R. Lieder, H. Jäger, H. Kämmerfing, M. Berst, D. Gutknecht, R. Henck, Nucl. Instrum. Methods Phys. Res. Sect. A: Accelerat. Spectrom. Detect. Assoc. Equip. **369**(1), 135 (1996). ISSN 0168-9002. https://www.sciencedirect.com/science/article/pii/0168900295007946
13. W. Mueller, J. Church, T. Glasmacher, D. Gutknecht, G. Hackman, P. Hansen, Z. Hu, K. Miller, P. Quirin, Nucl. Instrum. Methods Phys. Res. Sect. A: Accelerat. Spectrom. Detect. Assoc. Equip. **466**(3), 492 (2001). ISSN 0168-9002. https://www.sciencedirect.com/science/article/pii/S0168900201002571
14. J. Eberth, G. Pascovici, H. Thomas, N. Warr, D. Weisshaar, D. Habs, P. Reiter, P. Thirolf, D. Schwalm, C. Gund et al., Prog. Part. Nucl. Phys. **46**(1), 389 (2001). ISSN 0146-6410. https://www.sciencedirect.com/science/article/pii/S0146641001001454
15. N. Warr, J. van de Walle, M. Albers, F. Ames, B. Bastin, C. Bauer, V. Bildstein, A. Blazhev, S. Bönig, N. Bree et al., Eur. Phys. J. A **49**(3), 40 (2013). ISSN 1434-601X. https://doi.org/10.1140/epja/i2013-13040-9
16. A. Lopez-Martens, K. Hauschild, A. Korichi, J. Roccaz, J.P. Thibaud, Nucl. Instrum. Methods A **533**(3), 454 (2004)
17. R. Venturelli, D. Bazzacco, LNL Annu. Rep. **2004**, 220 (2005)
18. M. Berst, J. Eberth, H.M. Jäger, H. Kämmerling, R.M. Lieder, W. Renftle, Enclosure for a detector operating in an ultra-high vacuum (1995). https://patents.google.com/patent/WO1995003555A1/en
19. M. Berst, J. Eberth, H.M. Jäger, H. Kämmerling, R.M. Lieder, W. Renftle, Process for producing an encapsulated detector (1995). https://patents.google.com/patent/WO1995003556A1/en
20. P. Reiter, J. Eberth, H. Hess, S. Thiel, B. Pirard, J. Clauss, L. Delorenzi, M.O. Lampert, Receiving container for a detector which operates in an ultrahigh vacuum or in a protective gas atmosphere consisting of high-purity gas (2018). https://patents.google.com/patent/US10107923B2/en
21. D. Lersch, G. Pascovici, B. Birkenbach, B. Bruyneel, J. Eberth, H. Hess, P. Reiter, A. Wiens, H. Georg Thomas, Nucl. Instrum.

Methods Phys. Res. Sect. A: Accelerat. Spectrom. Detect. Assoc. Equip. **640**(1), 133 (2011). ISSN 0168-9002. https://www.sciencedirect.com/science/article/pii/S0168900211004591
22. G. Pascovici, A. Pullia, F. Zocca, B. Bruyneel, D. Bazzacco, WSEAS Trans. Circ. Syst. **7**(6), 470 (2008)
23. A. Pullia, G. Pascovici, B. Cahan, D.E. Weisshaar, C. Boiano, R. Bassini, M. Petcu, F. Zocca, IEEE Symp. Conf. Record Nucl. Sci. **3**, 1411 (2004)
24. F. Zocca, A. Pullia, D. Bazzacco, G. Pascovici, 2007 IEEE Nuclear Science Symposium Conference Record **1**, 7 (2007)
25. B. Bruyneel, B. Birkenbach, P. Reiter, Nucl. Instrum. Methods Phys. Res. Sect. A: Accelerat. Spectrom. Detect. Assoc. Equip. **641**(1), 92 (2011). ISSN 0168-9002. https://www.sciencedirect.com/science/article/pii/S0168900211006085
26. B. Birkenbach, B. Bruyneel, G. Pascovici, J. Eberth, H. Hess, D. Lersch, P. Reiter, A. Wiens, Nucl. Instrum. Methods Phys. Res. Sect. A: Accelerat. Spectrom. Detect. Assoc. Equip. **640**(1), 176 (2011). ISSN 0168-9002. https://www.sciencedirect.com/science/article/pii/S0168900211005912
27. A. Wiens, B. Birkenbach, B. Bruyneel, J. Eberth, H. Hess, G. Pascovici, P. Reiter, D. Bazzacco, E. Farnea, C. Michelagnoli et al., Eur. Phys. J. A **49**(4), 1 (2013)
28. B. Bruyneel, B. Birkenbach, J. Eberth, H. Hess, G. Pascovici, P. Reiter, A. Wiens, D. Bazzacco, E. Farnea, C. Michelagnoli et al., Eur. Phys. J. A **49**(5), 1 (2013)
29. B. Bruyneel, P. Reiter, A. Wiens, J. Eberth, H. Hess, G. Pascovici, N. Warr, D. Weisshaar, Nucl. Instrum. Methods Phys. Res. Sect. A: Accelerat. Spectrom. Detect. Assoc. Equip. **599**(2), 196 (2009). ISSN 0168-9002. https://www.sciencedirect.com/science/article/pii/S0168900208015921
30. B. Bruyneel, P. Reiter, A. Wiens, J. Eberth, H. Hess, G. Pascovici, N. Warr, S. Aydin, D. Bazzacco, F. Recchia, Nucl. Instrum. Methods Phys. Res. Sect. A: Accelerat. Spectrom. Detect. Assoc. Equip. **608**(1), 99 (2009). ISSN 0168-9002. https://www.sciencedirect.com/science/article/pii/S0168900209012455
31. V. Boldrini, G. Maggioni, S. Carturan, W. Raniero, F. Sgarbossa, R. Milazzo, D.R. Napoli, E. Napolitani, R. Camattari, D.D. Salvador, J. Phys. D: Appl. Phys. **52**(3), 035104 (2018). https://doi.org/10.1088/1361-6463/aae9c0
32. P.N. Peplowski, M. Burks, J.O. Goldsten, S. Fix, L.E. Heffern, D.J. Lawrence, Z.W. Yokley, Nucl. Instrum. Methods Phys. Res. Sect. A: Accelerat. Spectrom. Detect. Assoc. Equip. **942**, 162409 (2019). ISSN 0168-9002. https://www.sciencedirect.com/science/article/pii/S0168900219309842
33. L. Darken, Nucl. Instrum. Methods Phys. Res. Sect. B: Beam Interact. Mater. Atoms **74**(4), 523 (1993). ISSN 0168583X. https://linkinghub.elsevier.com/retrieve/pii/0168583X9395951Z
34. R.H. Pehl, N.W. Madden, J.H. Elliott, T.W. Raudorf, R.C. Trammell, L.S. Darken, IEEE Trans. Nucl. Sci. **26**(1), 321 (1979)
35. V. Boldrini, S.M. Carturan, G. Maggioni, E. Napolitani, D.R. Napoli, R. Camattari, D. De Salvador, Appl. Surf. Sci. **392**, 1173 (2017) ISSN 0169-4332. https://www.sciencedirect.com/science/article/pii/S0169433216320153
36. J. Poate, J.W. Mayer, Laser Annealing of Semiconductors, Vol. 22 (Elsevier, 1982). ISBN 9780125588201. https://linkinghub.elsevier.com/retrieve/pii/B978012558820 1X50017
37. R. Duffy, E. Napolitani, F. Cristiano, Laser Annealing Processes in Semiconductor Technology (Elsevier, 2021), pp. 175–250, ISBN 9780128202555. https://doi.org/10.1016/B978-0-12-820255-5.00007-6 https://linkinghub.elsevier.com/retrieve/pii/B9780128202555000076
38. D.D. Salvador, F. Sgarbossa, G. Maggioni, E. Napolitani, C. Carraro, S.M. Carturan, W. Raniero, S. Bertoldo, R. Milazzo, V. Boldrini et al., Proceedings **26**(1) (2019). ISSN 2504-3900. https://www.mdpi.com/2504-3900/26/1/39
39. E. Bruno, G.G. Scapellato, G. Bisognin, E. Carria, L. Romano, A. Carnera, F. Priolo, J. Appl. Phys. **108**(12) (2010). ISSN 00218979
40. C. Xu, C.L. Senaratne, J. Kouvetakis, J. Menéndez, Appl. Phys. Lett. **105**(23) (2014). ISSN 00036951
41. C. Carraro, R. Milazzo, F. Sgarbossa, D. Fontana, G. Maggioni, W. Raniero, D. Scarpa, L. Baldassarre, M. Ortolani, A. Andrighetto, et al., Appl. Surf. Sci. **509**(2019), 145229. ISSN 01694332 (2020). https://doi.org/10.1016/j.apsusc.2019.145229. https://linkinghub.elsevier.com/retrieve/pii/S0169433219340462
42. G. Maggioni, D. De Salvador, D. R. Napoli, E. Napolitani, P+ or n+ type doping process for semiconductors, WIPO Patent Application WO/2021/214028 (2021)
43. G. Maggioni, S. Carturan, W. Raniero, S. Riccetto, F. Sgarbossa, V. Boldrini, R. Milazzo, D.R. Napoli, D. Scarpa, A. Andrighetto et al., Eur. Phys. J. A **54**(3), 34 (2018). ISSN 1434-6001. http://link.springer.com/10.1140/epja/i2018-12471-0
44. E.L. Hull, R.H. Pehl, J.R. Lathrop, P.L. Mann, R.B. Mashburn, B.E. Suttle, H.S. Miley, C.E. Aalseth, T.W. Hossbach, 29th Monitoring Research Review: Ground-Based Nuclear Explosion Monitoring Technologies SEGMENTATION (2007)
45. G.S. King, F.T. Avignone, C.E. Cox, T.W. Hossbach, W. Jennings, J.H. Reeves, Nuclear Instruments and Methods in Physics Research, Section A: Accelerators, Spectrometers, Detectors and Associated Equipment **595**(3), 599 (2008), ISSN 01689002
46. S. Bertoldo, G. Maggioni, W. Raniero, C. Carraro, S. Riccetto, F. Sgarbossa, D. Scarpa, A. Andrighetto, A. Mazzolari, A. Gadea et al., Eur. Phys. J. A **57**(6), 1 (2021). ISSN 1434601X. https://doi.org/10.1140/epja/s10050-021-00487-8
47. W. Raniero, G. Maggioni, S. Bertoldo, S. Carturan, F. Sgarbossa, C. Carraro, E. Napolitani, D.R. Napoli, D.D. Salvador, Nuovo Cim. C **44**(4-5-5), 154 (2021)
48. Y.B. Gurov, V.S. Karpukhin, S.V. Rozov, V.G. Sandukovsky, D. Borowicz, J. Kwiatkowska, B. Rajchel, J. Yurkowski, Instrum. Exp. Tech. **52**(1), 137 (2009). ISSN 00204412
49. G. Maggioni, D.R. Napoli, J. Eberth, M. Gelain, S. Carturan, M.G. Grimaldi, S. Tatì, Eur. Phys. J. A **51**(11) (2015). ISSN 1434601X
50. S. Carturan, G. Maggioni, S.J. Rezvani, R. Gunnella, N. Pinto, M. Gelain, D.R. Napoli, Mater. Chem. Phys. **161**, 116 (2015). ISSN 02540584. https://doi.org/10.1016/j.matchemphys.2015.05.022
51. D.R. Napoli, G. Maggioni, S. Carturan, J. Eberth, V. Boldrini, D. De Salvador, E. Napolitani, P. Cocconi, G. Della Mea, M. Gelain et al., Acta Phys. Polon. B **48**(3), 387 (2017). ISSN 05874254
52. G. Maggioni, S. Carturan, L. Fiorese, N. Pinto, F. Caproli, D.R. Napoli, M. Giarola, G. Mariotto, Appl. Surface Sci. **393**, 119 (2017). ISSN 01694332. https://doi.org/10.1016/j.apsusc.2016.10.006
53. N. Pinto, F. Caproli, G. Maggioni, S. Carturan, D.R. Napoli, J. Non-Cryst. Solids **452**, 280 (2016). ISSN 00223093. https://doi.org/10.1016/j.jnoncrysol.2016.09.006
54. N. Pinto, F. Caproli, G. Maggioni, S. Carturan, D.R. Napoli, Mater. Sci. Semicond. Process. **74**(June 2017), 57 (2018). ISSN 13698001. https://doi.org/10.1016/j.mssp.2017.10.006
55. M. Gelain, D.R. Napoli, G. Maggioni, S. Carturan, J. Eberth, G. Della Mea, D. De Salvador, G. Mariotto, A. De Lorenzi, G. Valotto et al., Research and Development in HPGe Detectors at LNL. In: Proceedings of 10th Latin American Symposium on Nuclear Physics and Applications — PoS(X LASNPA) (Sissa Medialab, Trieste, Italy, 2014), December 2013, p. 042. https://pos.sissa.it/194/042